Prediction of the liquid-crystal phase behavior of hard right triangles from fourth-virial density-functional theories

Enrique Velasco*
Departamento de Física Teórica de la Materia Condensada, Instituto de Física de la Materia Condensada (IFIMAC) and Instituto de Ciencia de Materiales Nicolás Cabrera, Universidad Autónoma de Madrid, E-28049, Madrid, Spain

Yuri Martínez-Ratón†
Grupo Interdisciplinar de Sistemas Complejos (GISC), Departamento de Matemáticas, Escuela Politécnica Superior, Universidad Carlos III de Madrid, Avenida de la Universidad 30, E-28911, Leganés, Madrid, Spain

(Received 15 May 2023; accepted 19 June 2023; published 12 July 2023)

We have used an extended scaled-particle theory that incorporates four-body correlations through the fourth-order virial coefficient to analyze the orientational properties of a fluid of hard right isosceles triangles. This fluid has been analyzed by computer simulation studies, with clear indications of strong octatic correlations present in the liquid-crystal phase, although the more symmetric order tetratic phase would seem to be the most plausible candidate. Standard theories based on the second virial coefficient are unable to reproduce this behavior. Our extended theory predicts that octatic correlations, associated to a symmetry under global rotations of the oriented fluid by 45°, are highly enhanced, but not enough to give rise to a thermodynamically stable phase with strict octatic symmetry. We discuss different scenarios to improve the theoretical understanding of the elusive octatic phase in this intriguing fluid.

DOI: 10.1103/PhysRevE.108.014603

I. INTRODUCTION

Fluids of elongated particles in two dimensions (2D) [1] continue to unveil surprising behaviors [2]. Since the discovery of crystallization in hard-disc systems, fluids made of hard elongated particles, such as ellipsoids, have been seen to stabilize nematic phases with uniaxial symmetry [3]. As common in 2D, these phases possess quasi-long-range orientational order [4–6], but mean-field theories can still describe large regions where the tensor order parameter exhibits persistent values [7,8]. Since particles interact through purely overlap interactions, order in 2D phases made of hard elongated particles is solely governed by entropy, which shows here its most subtle nature.

More complicated 2D particle shapes have been explored more recently from a theoretical perspective [9–19], motivated by the possibility to fabricate colloidal particles of virtually any shape [20–22]. Particles with regular polygonal shapes have been demonstrated to exhibit mesophases [9,23], with 4-atic (or tetratic, with two directors and a global symmetry under rotation by 90°) phases for squares, 6-atic (with three directors and a symmetry under 60°) for equilateral triangles and hexagons. No further mesophases appear to get stabilized for polygonal shapes with more edges: They crystallize directly from the isotropic fluid through a KTHN-type transition, as in the case of discs [23,24]. Simulation of mixtures of particles has also found interesting behaviors [25].

Nonregular polygons open up exciting possibilities for further exploration [12,26]. Here, entropy plays an even more subtle role: Particles tend to form local clusters of oriented particles that can be viewed as superparticles, with symmetries sometimes very different from that of the monomers and therefore from the symmetry of the bulk liquid-crystal phase that would trivially follow from the monomers. Such is the case in fluids made of low-aspect-ratio rectangles, which tend to form highly stable square clusters that stabilize a global 4-atic phase [27]. The same behavior is found in vibrated monolayers of granular grains [28,29] and in experiments on colloidal particles [22]. Hard-kite-shaped particles have been studied by simulation [30] and theory [31], and 4-atic phases were also found. The basic understanding of this phase lies in the excluded area between particles (second-order virial coefficient), an essential ingredient of the scaled-particle theory (SPT) extension of classical Onsager theory. Three-body correlations can be incorporated into the theory through third-order virial coefficients [32], and the ensuing corrections are important: The stability region of the 4-atic phase is extended to larger aspect ratios and lower densities.

Recently, we studied a fluid made of hard right-angle isosceles triangles (HRTs) [33]. Motivated by Monte Carlo (MC) simulations by Gantapara *et al.* [34], we analyzed the fluid using standard SPT, based on the second virial coefficient (which is analytic), and an extension that includes the third-virial coefficient, calculated using MC integration. It turns out that none of these theories can reproduce the behavior predicted from the simulations: As the isotropic fluid is compressed, clustering of particles in clusters of var-

*enrique.velasco@uam.es
†yuri@math.uc3m.es

ious shapes give rise to strong 8-atic correlations, and an orientational distribution function with 4-atic symmetry but high secondary peaks at 45° with respect to the main peaks results. The equilibrium orientational distribution function from the theories, by contrast, shows no hint of high-order 8-atic symmetry.

The HRT fluid seems to be a unique case where an Onsager-type theory fails to give even a qualitative picture of a mesophase. In previous work, we have discussed this problem. On the one hand, the theory is strictly valid for infinitely long rods, while here we are considering particles of low aspect ratio. On the other, the sequence of virial coefficients in 2D fluids is known to have peculiar behavior, and the condition that scaled higher-order coefficients are small is not fulfilled. Finally, a crucial property of the HRT fluid and other 2D fluids made of hard polygonal particles is the strong clustering tendency of the fluid [12,33], with at least five types of clusters that form in the fluid at intermediate phases (before crystallization). Four of these clusters involve two particles (dimers), of square, triangular, and rhomboidal shapes (with two enantiomers in the latter case), and one involve four particles arranged in a square. The fluid can somehow be viewed as a multicomponent mixture of dynamic superparticles and might be more quantitatively described by association theories than by particle (monomer)-based theories. Before undertaking such a program, we speculated [12,33] that a theory based on four-body correlations (i.e., on the fourth virial coefficient) might give some indication as to whether high-order particle correlations, involved in clustering tendencies of the particles, might be important to understand the equilibrium structure of the fluid.

In the present paper, we show the predictions of such a theory. A resummed SPT is developed using the standard technique [32,33,35], which allows us to systematically incorporate an arbitrary number of virial coefficients. These objects are generalized virial coefficients in the sense that they are functionals of the orientational distribution function. The third and fourth virial coefficients are computed numerically, and the instability of the isotropic (I) phase against orientational orders of different symmetries is investigated. This process allows us to analyze the effect of increasing low order, from two- to four-particle correlations on the onset of bulk orientational order. Focusing on the 8-atic (or octatic) orientational symmetry, we explore the tendency of the fluid to stabilize orientational order through a bifurcation analysis. Our conclusion is that four-particle correlations do enhance octatic symmetry. More definite conclusions as to the orientational distribution of particles would require a full minimization of the free energy. However, a more quantitative theory should incorporate particle clustering [33], which is not possible with the present SPT scheme, and further studies will have to wait until a proper treatment of clusters can be formulated.

The paper is organized as follows. In Sec. II, we present the theory and a method to extend SPT to include the fourth virial coefficient. Also, we provide some details on the numerical calculation of this coefficient. In Sec. III, we present the results, along with the results obtained from extrapolations of virial coefficients and resummations of the virial theory in the isotropic phase, which may help to explain the role of many-particle correlations. Some conclusions are drawn in Sec. IV. The Appendices collect some further numerical details and additional results.

II. THEORY

Our theory uses the same strategy followed in our previous works on the third virial coefficient [32,33], but now the theory is extended to an arbitrary number of virial coefficients. We start from the following analytic expression for the equation of state, valid for a fluid of oriented particles:

$$\beta pa = \frac{\eta}{1-\eta} + \frac{\sum_{k=2}^{n} c_k[h]\eta^k}{(1-\eta)^q}. \tag{1}$$

The parameter q in Eq. (1) controls the divergence of the second term at close packing, $\eta = \eta_{\rm cp} \equiv 1$. It is taken as a free parameter and will be important to compare the resulting equation of state with MC simulations. $\eta = \rho a$ is the packing fraction, with ρ and a the number density and particle area, respectively. $h(\phi)$ is the orientational distribution function, which quantifies the average orientation of the particles, where ϕ is the angle between the averaged orientation of the main symmetry axis of a typical particle and the main director. This function is normalized,

$$\int_0^{2\pi} d\phi h(\phi) = 1. \tag{2}$$

The coefficients $c_n[h]$ are functionals of the orientational distribution function and can be related to the standard virial coefficients by equating the low-density expansion of (1) with the exact virial expansion up to nth order (note that the expansion in Eq. (1) is truncated at this order),

$$c_n[h] = b_n[h] + \sum_{k=1}^{n-2}(-1)^k \binom{q}{k} b_{n-k}[h], \tag{3}$$

where we have defined

$$b_n[h] \equiv \frac{B_n[h]}{a^{n-1}} - 1, \tag{4}$$

with $B_n[h]$ the standard nth virial coefficient. Note that these coefficients are also functionals of $h(\phi)$. Fixing $q = 0$ in Eq. (1), the exact virial expansion up to the nth order is recovered. Also, selecting $q = 2$ and $n = 2$, we obtain the SPT approximation, while for the same q and $n = 3$ the equation of state turns out to be the same as the one used in Ref. [33] to study fluid orientational ordering close to the I-p–atic bifurcation point, henceforth called B_3-SPT. This shows that Eq. (1) is a versatile starting point to explore nonstandard approximations to the equation of state of oriented fluids in 2D.

In this paper, we start by exploring the case $q = 2$ and $n = 4$ (henceforth called B_4-SPT), and then use extrapolated values for the first three virial coefficients, B_2, B_3, and B_4 of the I phase to predict the value of B_5, giving rise to the B_5^*-SPT theory (the asterisk denotes an extrapolated value for B_5). Not only are the values of the virial coefficients for the completely disordered fluid calculated but also relevant Fourier components with respect to weak orientational order of particular p-atic symmetries. This allows for a bifurcation analysis of the I phase with respect to these symmetries. Finally, the effect of q has also been assessed for $n = 3, 4$, and

5, which can be used to explore the effect of the divergence of the equation of state on the relative locations of the I-2–atic and I-8-atic bifurcations, and, in general, on the performance of the theory when compared with MC simulations.

To proceed, we first need to derive the free energy. As usual, it is more convenient to obtain the excess free energy by integrating the excess pressure, which can be written as $\beta p_{\rm exc} a = \beta p a - \eta$ ($\beta p_{\rm id} = \rho$ is the ideal pressure). Using the thermodynamic relation $\beta p_{\rm exc} a = \eta^2 \frac{\partial \varphi_{\rm exc}}{\partial \eta}$, with $\varphi_{\rm exc}$ the excess part of the Helmholtz free-energy per particle, we can integrate the expression above with respect to η to obtain

$$\varphi_{\rm exc}[h] = -\log(1-\eta) + \sum_{k=2}^{n} c_k[h]\, {}_2F_1(k-1, q; k; \eta)\frac{\eta^{k-1}}{k-1}. \tag{5}$$

The integration constant was set to zero to ensure that the excess free energy be zero at the low-density limit. ${}_2F_1$ is the hypergeometric function:

$${}_2F_1(n, q; n+1; \eta)\frac{\eta^n}{n} = \int_0^\eta \frac{u^{n-1}}{(1-u)^q} du. \tag{6}$$

The ideal part of the free energy per particle has the exact form

$$\varphi_{\rm id}[h] = \log\eta - 1 + \int_0^{2\pi} d\phi h(\phi)\log(2\pi h(\phi)), \tag{7}$$

giving the total free-energy functional as $\varphi[h] = \varphi_{\rm id}[h] + \varphi_{\rm exc}[h]$.

Since we will only be interested in assessing the contribution of higher-order correlations to the stability of the I phase against p-atic symmetries, we restrict here to a stability analysis of the functional against orientational fluctuations of a given symmetry. In practice, this means that the full Fourier expansion of $h(\phi)$ can be truncated, keeping only the term with the required symmetry. More specifically, close to the I-2m-atic ($m = 1, \ldots, 4$) bifurcation point, we approximate

$$h(\phi) \simeq \frac{1}{2\pi}[1 + h_m \cos(2m\phi)], \tag{8}$$

with h_m the first Fourier amplitude with mth symmetry. Explicitly, $m = 1$ ($2-$atic), 2 ($4-$atic), 3 ($6-$atic), and 4 ($8-$atic). Inserting this expression in the total free-energy functional $\varphi[h]$, we obtain, to lowest order in h_m,

$$\varphi[h] = \varphi_{\rm I} + \Delta\varphi[h], \tag{9}$$

where

$$\varphi_{\rm I} = \log\left(\frac{\eta}{1-\eta}\right) - 1 + \sum_{k=2}^{n} \mathcal{C}_k^{(0)}[h]\frac{\eta^{k-1}}{k-1}\, {}_2F_1(k-1, q; k; \eta) \tag{10}$$

is the free energy of the I phase, and

$$\Delta\varphi[h] = \frac{h_m^2}{2}\chi_m(\eta),\ m \geqslant 1, \tag{11}$$

with

$$\chi_m(\eta) = 1 + 2\sum_{k=2}^{n} \frac{\mathcal{C}_k^{(m)}\eta^{k-1}}{(k-1)!}\, {}_2F_1(k-1, q; k; \eta),$$
$$m = 1, \ldots, 4, \tag{12}$$

TABLE I. Values of the packing fractions η_n at I-2-atic ($n = 1$), I-4-atic ($n = 2$), I-6-atic ($n = 3$), and I-8-atic ($n = 4$) bifurcations from the SPT, B_3-SPT, and B_4-SPT theories, and from the truncated virial expansions B_4 and B_5^*.

Bifurcation	I-2-atic	I-4-atic	I-6-atic	I-8-atic
η_n from SPT	0.8249	0.9928	0.9821	0.9444
η_n from B_3-SPT	0.7325	0.9794	0.9328	0.8353
η_n from B_4-SPT	0.7281	0.9681	0.8631	0.7399
η_n from B_5^*-SPT	0.7255	0.9590	0.8304	0.7091
η_n from B_4	1.0038	3.3121	1.8485	1.2049
η_n from B_5^*	0.8715	2.1817	1.3071	0.9326

being the extra contribution associated to an orientational fluctuation with symmetry of order m and amplitude h_m. In the expressions above, we have defined

$$\mathcal{C}_n^{(m)} = \mathcal{B}_n^{(m)} + \sum_{k=1}^{n-2}(-1)^k \binom{q}{k} \mathcal{B}_{n-k}^{(m)}, \tag{13}$$

while the coefficients $\mathcal{B}_n^{(m)}$ denote the Fourier components of the scaled virial coefficients. To quadratic order:

$$b_n[h] = \mathcal{B}_n^{(0)} + \frac{h_m^2}{2}\mathcal{B}_n^{(m)}. \tag{14}$$

The procedures used to calculate the $\mathcal{B}_n^{(m)}$ coefficients are described in Appendix A, while the numerical values for the bifurcations are discussed in Sec. III. We only note here that, to find the value of packing fraction η_m for the I-2m-atic bifurcation, we need to solve the equation $\chi_m(\eta) = 0$.

In this paper, we limit the maximum order of the virial coefficient to $m = 4$. However, it will be worthwhile to explore the effect of an extrapolated fifth and possibly higher-order virial coefficients. From Eq. (1) with $n = 4$ we can obtain the relation between $b_m[h]$ for $m \geqslant 5$ and $b_2[h]$, $b_3[h]$, and $b_4[h]$:

$$\begin{aligned} b_m[h] = \{&2(m-2)(m-3)b_4[h] \\ &- 2(m-2)(m-4)(q-1)b_3[h] \\ &+ (m-3)(m-4)(q-1)(q-2)b_2[h]\} \\ &\times \frac{q(q+1)\cdots(q+m-5)}{2(m-2)!}. \end{aligned} \tag{15}$$

III. RESULTS

We start by comparing the values of packing fraction at the bifurcations from the I phase to the different p-atic phases, using an extended SPT with increasing number of virial coefficients. Table I presents the results. Except B_5^*-SPT (which is based on an extrapolated fifth virial coefficient), all of the theories predict a first bifurcation to the 2-atic phase. However, the next bifurcation is invariably the $\mathrm{I}-8$-atic bifurcation, which shows the tendency of the HRT fluid to develop octatic correlations. Also, the difference $\Delta\eta \equiv \eta_4 - \eta_1$ between the $\mathrm{I}-8$-atic and $\mathrm{I}-2$-atic bifurcations tends to dramatically decrease when the theory is extended with the fourth virial coefficient (cf. $\Delta\eta = 0.1195$ for the standard SPT, based on the second virial coefficient, with $\Delta\eta = 0.0118$ for B_4-SPT, but with the difference between the B_3-SPT and standard SPT,

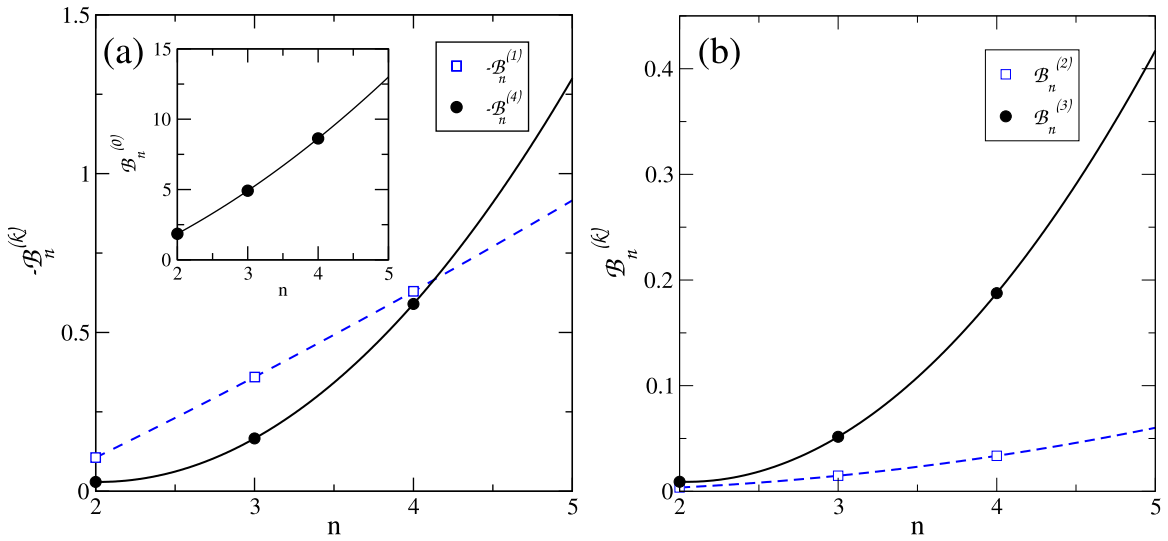

FIG. 1. Virial Fourier components $\mathcal{B}_n^{(k)}$ for $k = 1, 4$ (a) (the inset shows the case $k = 0$) and $k = 2, 3$ (b) together with parabolic extrapolation to $n = 5$.

$\Delta\eta = 0.1028$, hardly changing). This clearly demonstrates the importance of four-particle correlations in this system. These correlations are involved in the formation of very stable tetramers of triangles with square shape, which may dominate the properties of the system at high densities.

The HRT fluid has been examined in detail by Gantapara *et al.* [34] using MC simulation. This paper predicts a first-order phase transition from the I phase to a 4-atic liquid-crystal phase. Our own simulations [33] indicate that the nature of the liquid-crystal phase strongly depends on the protocol (either compression or expansion) and starting configurations used in the simulations, to the extent that the equilibrium configurations may exhibit strong octatic or purely tetratic correlations. The value of the packing fraction at which the I phase changes to the liquid-crystal phase was obtained to be $\eta = 0.733$. From Table I, we can see that the B_4-SPT approximation is very good at predicting the correct density. Whether the symmetry of the liquid-crystal phase is tetratic or octatic is a more delicate question that demands further analysis. Note that the predicted values for $\eta_2 \sim 1$ are large in all cases due to the small values of the $\mathcal{B}_n^{(2)}$ coefficients. This may indicate that the I-4-atic transition is of first order, as shown in Appendix B in the framework of SPT.

To complete the picture, we have also calculated the bifurcations using truncated virial expansions instead of the resummed virial series based on the SPT approximation. The results are shown in Table I. In common with the standard Onsager-like theories for low aspect-ratio particles in 2D, the values of packing fractions are absurdly large and generally unphysical for the theories based on B_2 and B_3 virial coefficients (not shown). But this is because density correlations are too grossly represented, while angular correlations are expected to be more faithfully captured by the virial coefficients. Therefore, the trends in packing fraction values as more virial coefficients are added may be relevant. In line with the SPT-based theories, the bifurcation of the I − 8-atic transition becomes closer to the I − 2-atic bifurcation as more virial coefficients are added, again demonstrating the importance of the higher (especially the fourth) virial coefficients to represent the structure of the HRT fluid.

To further explore the effect of higher-order virial coefficients, we have obtained extrapolated values for the fifth virial coefficient. Note that even though the third- and fourth-order virial coefficients are obtained numerically with a numerical effort which is acceptable, the fifth virial coefficient is much harder to obtain (especially their necessary Fourier projections are highly fluctuating with the relative angle between particles and require very detailed and costly MC integrations). Therefore, we simply extrapolate the lower-order coefficients. This is shown in Fig. 1, where the values of $\mathcal{B}_n^{(k)}$, for $n = 2, 3$, and 4, and $k = 0, \cdots, 4$, are shown. We can see that all the absolute values of the coefficients are increasing functions of n. The figures include parabolic interpolations to the data. We take the corresponding extrapolations up to $n = 5$ and examine the consequences. Coming back to the bifurcation densities, we see from Table I that the trend for $\Delta\eta$ as more virial coefficients are taken into account continues to be decreasing, actually becoming negative. This indicates that fifth-order correlations further promote octatic ordering. This is just a trend, since the extrapolated values for $\mathcal{B}_4^{(k)}$, and the resulting B_5^*-SPT theory, need not be accurate. The conclusion is the same if one looks at the truncated virial series results, Table I, with $\eta_2 < \eta_4$ but very close. As a side comment, it is interesting that the first two bifurcations of the truncated virial expansion of the fifth order are at physical packing fraction values (i.e., below unity), in contrast to the lower-order expansions.

We now turn to a discussion on the thermodynamics of the different approximations by examining the equation of state in the I phase. In the results presented above, the exponent q was set to a value of 2. Now we consider flexible choices for q and examine the consequences for the equation of state in the whole range of densities. In all cases, we compare with the

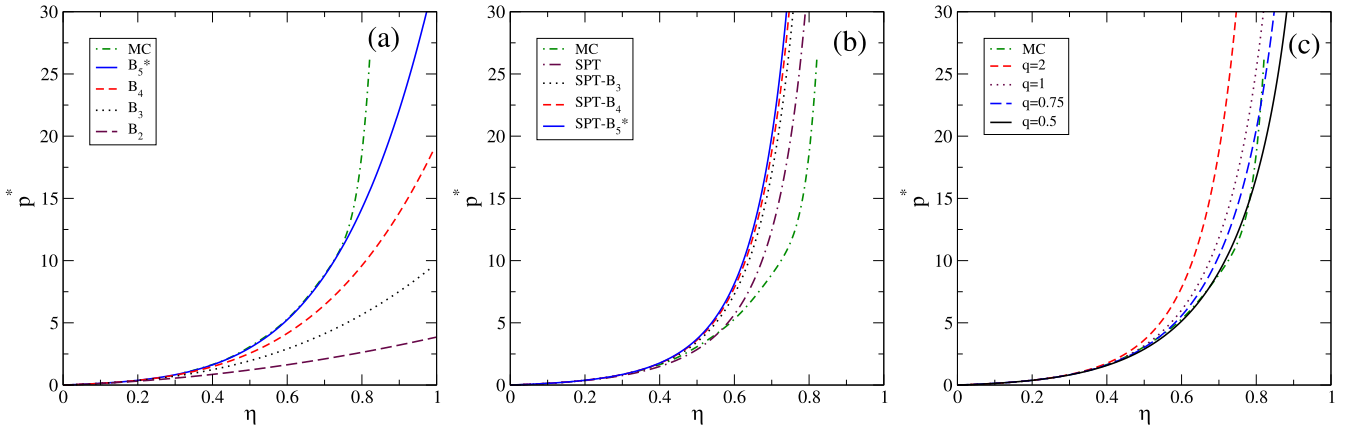

FIG. 2. (a) Equations of state from the second, third, fourth, and fifth virial expansions. (b) Equations of state from Eq. (1) selecting $q = 2$ and fixing the correct virial coefficients up to second, third, fourth and fifth orders (the latter using its extrapolated value). (c) Equations of state from Eq. (1) using the correct B_n ($n = 2, \ldots, 4$) and using different values of q.

MC results of Gantapara *et al.* [34] from the compression runs (these data have been digitized from the original article and presented as a smooth curve to aid in visualizing the data in comparison with the different theoretical equations of state).

Figure 2 presents the equations of state in the I phase for different theories and also with different values of q. Note that, according to the simulations, the I phase is stable up to $\eta = 0.733$, but the compression results from the simulations could be taken as reproducing a metastable I phase beyond the liquid-crystal transition. As we have shown previously [33], the structure of the fluid in this regime appears to be quite complex, with different clusters of particles, which give rise to sampling problems in the simulations. Therefore, the comparison beyond this density should be taken with caution, but we extend the density interval shown in the figures to assess the impact of different diverging behaviors.

We start by looking at Fig. 2(a), which shows the equations of state from truncated virial expansion. As expected, the addition of more virial coefficients improve the results (note that only the $\mathcal{B}_n^{(0)}$ coefficients are needed in the I phase). But it is remarkable that the expansion based on B_5^* is very accurate in the whole density interval where the I phase is stable. Clearly, the addition of the extrapolated fifth virial coefficient corrects almost completely the equation of state, which demonstrates that the extrapolation may be accurate.

Let us consider the equations of state as derived from the resummed expansions based on SPT, i.e., selecting $q = 2$. This is shown in Fig. 2(b). Although the pressure is correctly reproduced at moderate densities by all theories, the results are somewhat disappointing at high density when they are compared with the simulations. This is otherwise expected, as resummed theories are known to be relatively accurate in predicting densities of phase transitions to liquid-crystal phases, but not so in reproducing the equations of state quantitatively.

Finally, we present an investigation which aims to explore the effect of different diverging behaviors of the equation of state on the pressure and the bifurcation points. This is controlled by the parameter q introduced in Eq. (1). We present some results for the cases $q = 0.5$, 0.75, and 1. Figure 2(c) show the equations of state for these cases. Clearly, as q is decreased the results improve significantly. The best quantitative agreement is obtained for $q = 0.5$.

The changes in the bifurcation points are shown in Fig. 3, which are focused on the I-2-atic and and I-8-atic bifurcations, represented by η_1 and η_4, respectively. In the different panels, we represent the variations of both parameters as q is changed within a wide interval, for the three resummed theories incorporating the third, fourth, and (extrapolated) fifth virial coefficients. The crossover between η_1 and η_4 is induced as q increases, but the crossover value decreases with the order of the theory. Note that, for the B_4-SPT theory, the critical value of q is close to 2. Note that an optimal equation of state requires values of q which are not optimal for the bifurcation point, but the inclusion of higher virial coefficients may improve this situation, as shown by the resummed theory based on an extrapolated fifth virial coefficient.

IV. CONCLUSIONS

In this paper, we have examined the effect of the high-order virial coefficients on the structure and thermodynamics of the HRT fluid. Virial coefficients and relevant Fourier projections up to fourth order have been evaluated by MC integration. In addition, the fifth-order virial coefficient has been extrapolated. When compared to simulations, the fifth-order truncated virial expansion, which requires the extrapolated value of the zeroth-order Fourier component $\mathcal{B}_5^{(0)}$, gives a good approximation for the equation of state of the I phase up to a packing fraction of $\eta \simeq 0.75$. Note that this is slightly beyond the predicted range of stability for the I phase before the liquid-crystal phase becomes stable. In addition, it is the lowest-order truncated virial expansion for which the I-2-atic and I-8-atic bifurcation points occur at packing fractions below unity. The resummed B_n-SPT approaches overestimate the pressure, but packing fractions at bifurcation are correct as compared with simulation for $n > 2$. To investigate the impact of different diverging behaviors of the equation of state, we explored values of the exponent q different from the standard choice $q = 2$. As q is decreased from 1 to 0.5, the resulting equation of

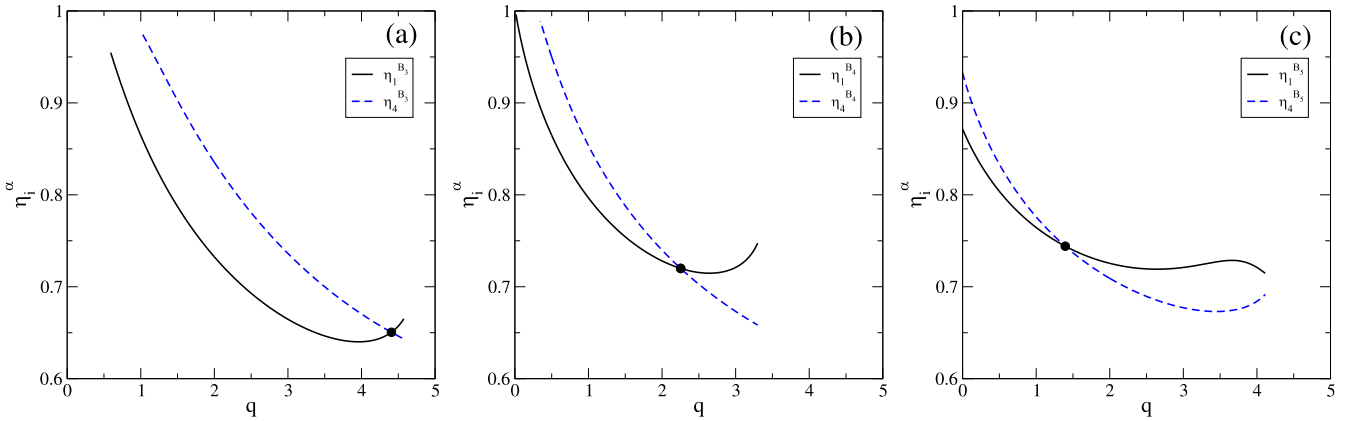

FIG. 3. Packing fractions $\eta_1(q)$ and $\eta_4(q)$ resulting from (a) B_3-SPT, (b) B_4-SPT, and (c) B_5^*-SPT theories. In all cases, the bifurcation condition $\chi_n(\eta) = 0$ has been applied.

state compares quite reasonably with simulation. However, the values of the bifurcation packing fractions η_1 and η_4 deviate quite significantly from simulation, and the difference $\Delta\eta = \eta_4 - \eta_1$ increases as q decreases.

As far as the resummed theories are concerned, the B_4-SPT theory gives $\eta_1 \lesssim \eta_4$, while the B_5^*-SPT theory (with an extrapolated fifth virial coefficient) already predicts $\eta_1 > \eta_4$. The crossover point is located between $q = 1$ and 1.5, which in turn implies that the equation of state will be better than in the standard case. An obvious outcome of this investigation is that minor changes in the form of the equation of state may have important quantitative consequences. Overall, the results presented in this paper point to the necessity to include virial coefficients beyond the fourth if the equation of state and the I-8-atic bifurcation point are to be reproduced correctly. Unfortunately, such an effort would incur a high computational cost, rendering the approach based on Eq. (1) impractical. Clearly, an alternative approach is needed to explain the behavior of the HRT fluid and the correct symmetry of its liquid-crystal phase. We are inclined to believe that this theory should include the effect of particle clustering into superparticles, such as square tetramers obtained by joining four triangular monomers. These square-shaped configurations will certainly stabilize the tetratic phase, while other clusters such as square dimers, in equilibrium with tetramers, will produce octatic correlations.

ACKNOWLEDGMENTS

Financial support from Grant No. PID2021-126307NB-C21 (MCIU/AEI/FEDER,UE) is acknowledged.

APPENDIX A: FOURIER COMPONENTS OF VIRIAL COEFFICIENTS

In this Appendix, we give details on the calculation of the Fourier components of the virial coefficients $B_n[h]$, $n = 2, \ldots, 4$. These components are needed in the analysis of the bifurcation points from the I fluid to the p–atic phase. The virial coefficients are, in general, functionals of the orientational distribution function $h(\phi)$ and can be written in the usual diagrammatic form as [36]

$$-2B_2[h]A =$$ 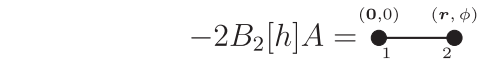 (A1)

$$-3B_3[h]A =$$ 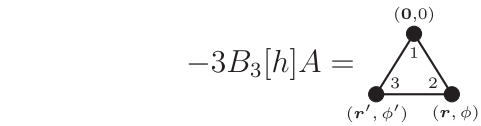 (A2)

$$-4B_4[h]A = \frac{3}{2}$$ 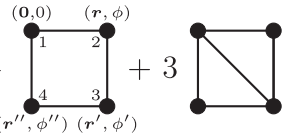 $$+ 3$$ $$+ \frac{1}{2}$$ 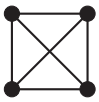 (A3)

Nodes and bonds label particles and Mayer functions, respectively. The reference system is located at node 1, which means that its position and angle are $(\boldsymbol{r}_1, \phi_1) = (\boldsymbol{0}, 0)$. Therefore, the nodes labeled as 2–4 (in a clockwise direction) have relative coordinates $\boldsymbol{r}_2 - \boldsymbol{r}_1 \equiv \boldsymbol{r}$, $\boldsymbol{r}_3 - \boldsymbol{r}_1 \equiv \boldsymbol{r}'$, $\boldsymbol{r}_4 - \boldsymbol{r}_1 \equiv \boldsymbol{r}''$, $\phi_2 - \phi_1 \equiv \phi$, $\phi_3 - \phi_1 \equiv \phi'$, $\phi_4 - \phi_1 \equiv \phi''$. The spatial and angular integrations with respect to $\boldsymbol{r}_1$ and ϕ_1 in $B_n[h]$ can then be performed trivially. In particular, a factor equal to the total area A cancels out, see Eqs. (A1)–(A3). Integration over ϕ_1 allows us to define the following angular functions:

$$\Psi_2(\phi) \equiv \int_0^{2\pi} d\phi_1 h(\phi_1) h(\phi_1 + \phi), \tag{A4}$$

$$\Psi_3(\phi, \phi') \equiv \int_0^{2\pi} d\phi_1 h(\phi_1) h(\phi_1 + \phi) h(\phi_1 + \phi'), \tag{A5}$$

$$\Psi_4(\phi, \phi', \phi'') \equiv \int_0^{2\pi} d\phi_1 h(\phi_1) h(\phi_1 + \phi) \times h(\phi_1 + \phi') h(\phi_1 + \phi''), \tag{A6}$$

Close to the I-2n-atic bifurcation point, we can approximate $h(\phi)$, up to first order, as

$$h(\phi) \simeq \frac{1}{2\pi}[1 + h_n \cos(2n\phi)], \quad n = 1, \ldots, 4. \tag{A7}$$

To lowest order, the angular functions become

$$\Psi_2(\phi) = \frac{1}{2\pi}\left\{1 + \frac{h_n^2}{2}\cos(2n\phi)\right\}, \tag{A8}$$

$$\Psi_3(\phi,\phi') = \frac{1}{(2\pi)^2}\left\{1 + \frac{h_n^2}{2}[\cos(2n\phi) + \cos(2n\phi') + \cos(2n\phi)\cos(2n\phi')]\right\}, \tag{A9}$$

$$\Psi_4(\phi,\phi',\phi'') = \frac{1}{(2\pi)^3}\left\{1 + \frac{h_n^2}{2}[\cos(2n\phi) + \cos(2n\phi') + \cos(2n\phi'') + \cos(2n\phi)\cos(2n\phi') + \cos(2n\phi)\cos(2n\phi'') + \cos(2n\phi')\cos(2n\phi'')]\right\}. \tag{A10}$$

The spatial integrals involved in $B_n[h]$ can be defined to be angular kernels,

$$\mathcal{K}_2(\phi) = -\frac{1}{2}\int d\boldsymbol{r} f(\boldsymbol{r},\phi), \tag{A11}$$

$$\mathcal{K}_3(\phi,\phi') = -\frac{1}{3}\int d\boldsymbol{r}\int d\boldsymbol{r}' f(\boldsymbol{r},\phi)f(\boldsymbol{r}',\phi')f(\boldsymbol{r}-\boldsymbol{r}',\phi-\phi'), \tag{A12}$$

$$\mathcal{K}_4^{(1)}(\phi,\phi',\phi'') = -\frac{3}{8}\int d\boldsymbol{r}\int d\boldsymbol{r}'\int d\boldsymbol{r}'' f(\boldsymbol{r},\phi)f(\boldsymbol{r}'',\phi'')f(\boldsymbol{r}-\boldsymbol{r}',\phi-\phi')f(\boldsymbol{r}'-\boldsymbol{r}'',\phi'-\phi''), \tag{A13}$$

$$\mathcal{K}_4^{(2)}(\phi,\phi',\phi'') = -\frac{3}{4}\int d\boldsymbol{r}\int d\boldsymbol{r}'\int d\boldsymbol{r}'' f(\boldsymbol{r},\phi)f(\boldsymbol{r}',\phi')f(\boldsymbol{r}'',\phi'')f(\boldsymbol{r}-\boldsymbol{r}',\phi-\phi')f(\boldsymbol{r}'-\boldsymbol{r}'',\phi'-\phi''), \tag{A14}$$

$$\mathcal{K}_4^{(3)}(\phi,\phi',\phi'') = -\frac{1}{8}\int d\boldsymbol{r}\int d\boldsymbol{r}'\int d\boldsymbol{r}'' f(\boldsymbol{r},\phi)f(\boldsymbol{r}',\phi')f(\boldsymbol{r}'',\phi'')f(\boldsymbol{r}-\boldsymbol{r}',\phi-\phi')f(\boldsymbol{r}'-\boldsymbol{r}'',\phi'-\phi'')f(\boldsymbol{r}-\boldsymbol{r}'',\phi-\phi''). \tag{A15}$$

Note that $\mathcal{K}_2(\phi)$ is just half the excluded area. The superindex m in the definition of $\mathcal{K}_4^{(m)}(\cdots)$ labels the empty square-diagram ($m=1$), the square-diagram with one diagonal ($m=2$), and the square-diagram with two diagonals ($m=3$), respectively. To implement the bifurcation analysis, we need the following Fourier components of these kernels:

$$\mathcal{K}_{2,n} = \int_0^{2\pi} d\phi\cos(2n\phi)\mathcal{K}_2(\phi), \tag{A16}$$

$$\mathcal{K}_{3,n,m} = \int_0^{2\pi} d\phi\cos(2n\phi)\int_0^{2\pi} d\phi'\cos(2m\phi')\mathcal{K}_3(\phi,\phi'), \tag{A17}$$

$$\mathcal{K}_{4,n,m,l}^{(k)} = \int_0^{2\pi} d\phi\cos(2n\phi)\int_0^{2\pi} d\phi'\cos(2m\phi')\int_0^{2\pi} d\phi''\cos(2l\phi'')\mathcal{K}_4^{(k)}(\phi,\phi',\phi''). \tag{A18}$$

Finally, the virial coefficients $B_n[h]$ can be approximated, close to the bifurcation point, by using Eqs. (A1)–(A3), (A8)–(A10), and (A11)–(A15), as

$$\begin{aligned}
B_2[h] &= \prod_{k=1}^{2}\left(\int_0^{2\pi} d\phi_k h(\phi_k)\right)\mathcal{K}_2(\phi) = \int_0^{2\pi} d\phi\Psi_2(\phi)\mathcal{K}_2(\phi) = B_2^{(0)} + \frac{h_n^2}{2}B_2^{(n)},\\
B_3[h] &= \prod_{k=1}^{3}\left(\int_0^{2\pi} d\phi_k h(\phi_k)\right)\mathcal{K}_3(\phi,\phi') = \int_0^{2\pi} d\phi\int_0^{2\pi} d\phi'\Psi_3(\phi,\phi')\mathcal{K}_3(\phi,\phi') = B_3^{(0)} + \frac{h_n^2}{2}B_3^{(n)},\\
B_4[h] &= \prod_{k=1}^{4}\left(\int_0^{2\pi} d\phi_k h(\phi_k)\right)\left(\sum_{m=1}^{3}\mathcal{K}_4^{(m)}(\phi,\phi',\phi'')\right)\\
&= \int_0^{2\pi} d\phi\int_0^{2\pi} d\phi'\int_0^{2\pi} d\phi''\Psi_4(\phi,\phi',\phi'')\left(\sum_{m=1}^{3}\mathcal{K}_4^{(m)}(\phi,\phi',\phi'')\right) = B_4^{(0)} + \frac{h_n^2}{2}B_4^{(n)},
\end{aligned} \tag{A19}$$

with

$$B_2^{(0)} = \frac{\mathcal{K}_{2,0}}{2\pi}, \quad B_2^{(n)} = \frac{\mathcal{K}_{2,n}}{2\pi}, \quad B_3^{(0)} = \frac{\mathcal{K}_{3,0,0}}{(2\pi)^2}, \quad B_3^{(n)} = \frac{1}{(2\pi)^2}(2\mathcal{K}_{3,n,0} + \mathcal{K}_{3,n,n}), \quad B_4^{(0)} = \frac{1}{(2\pi)^3}\sum_{m=1}^{3}\mathcal{K}_{4,0,0,0}^{(m)},$$

$$B_4^{(n)} = \frac{1}{(2\pi)^3}\left\{\sum_{m=1}^{2}\left[2\mathcal{K}_{4,n,0,0}^{(m)} + \mathcal{K}_{4,0,n,0}^{(m)} + 2\mathcal{K}_{4,n,n,0}^{(m)} + \mathcal{K}_{4,n,0,n}^{(m)}\right] + 3\left[\mathcal{K}_{4,n,0,0}^{(3)} + \mathcal{K}_{4,n,n,0}^{(3)}\right]\right\}. \tag{A20}$$

TABLE II. Values of the coefficients $\mathcal{B}_k^{(n)}$, obtained analytically for $k = 2$ from Eq. (A22), and numerically from MC integration and Gaussian quadrature for $k > 2$.

k	$\mathcal{B}_k^{(0)}$	$\mathcal{B}_k^{(1)}$	$\mathcal{B}_k^{(2)}$	$\mathcal{B}_k^{(3)}$	$\mathcal{B}_k^{(4)}$
2	1.8552	−0.1061	−0.0036	−0.0091	−0.0294
3	4.9158	−0.3597	−0.0148	−0.0516	−0.1662
4	8.6307	−0.6296	−0.0336	−0.1876	−0.5897

From these approximations, we define the scaled Fourier components of the virial coefficients:

$$\mathcal{B}_k^{(0)} \equiv \frac{B_k^{(0)}}{a^{k-1}} - 1, \quad \mathcal{B}_k^{(n)} \equiv \frac{B_k^{(n)}}{a^{k-1}}. \tag{A21}$$

The second-order coefficients $\mathcal{B}_2^{(n)}$ can be calculated analytically:

$$\mathcal{B}_2^{(n)} = -\frac{8}{\pi(4n^2-1)} \cos^2\left[\frac{(2n-1)\pi}{8}\right] \cos^2\left[\frac{(2n+1)\pi}{8}\right]. \tag{A22}$$

The remaining coefficients have to be computed numerically. We have used MC integration for the spatial integrals and Gaussian quadratures for the angular integrals, using special tricks to deal with the rapidly varying trigonometric functions of high index. 10^8 configurations were used to evaluate the spatial integrals. The results are collected in Table II.

APPENDIX B: RELATIVE STABILITY OF THE 4–ATIC PHASE

For those nth virial theories which predict an I-2–atic bifurcation below the I-8–atic, one may wonder which of the following scenarios takes place at densities above the I-8–atic bifurcation: (i) the 8-atic and 2-atic free-energy branches cross each other at some density or (ii) the 2–atic branch continues to be the lowest one. To investigate this point, we have minimised the B_2-SPT functional, considering a subset of Fourier coefficients $\{h_k\}$ with $k = 4j$:

$$h(\phi) = \frac{1}{2\pi}\left[1 + \sum_{k=0}^{n_{\max}} h_k \cos(2k\phi)\right]. \tag{B1}$$

This choice gives a distribution $h(\phi)$ with perfect 8-atic symmetry. A free-energy branch was generated for a density interval starting at the I-8-atic bifurcation point and up to densities such that the 8-atic order parameter is $Q_8 \simeq 0.97$ (we checked that with this condition the truncated Fourier series still gives correct results). The 2–atic branch was also calculated up to densities such that $Q_2 \simeq 0.97$. Figure 4(a) shows the free-energy differences $\Delta\varphi \equiv \varphi_\alpha - \varphi_I$ ($\alpha = 2,6,8$–atic) between α and I phases calculated from their respective bifurcation points. As expected, the 8-atic branch is always metastable. However, the results indicate that the first scenario above can be discarded, as the difference between the 8-atic and 2-atic free-energy branches is huge (note that the latter bifurcates from the isotropic at a much lower density). The situation is even worse in the case of the metastable 6-atic phase, as it bifurcates at even higher packing fractions (see Table I). We note that the 4-atic phase also bifurcates from the I phase but, unlike the 2-atic, 8-atic, and 6-atic phases, it does so via a first-order transition. This can be demonstrated, not via Fourier-amplitude minimization (we were unable to obtain a metastable 4-atic solution with the proper restrictions over $\{h_k\}$), but from a simple one-parameter minimization of the orientation distribution:

$$h(\phi) = \frac{e^{\lambda\cos(2n\phi)}}{2\pi I_0(\lambda)}, \quad \phi \in [0, 2\pi], \quad n = 1, \cdots, 4. \tag{B2}$$

$I_0(x)$ is the zeroth-order modified Bessel function of the first kind,and λ is a variational parameter. The results are shown in Fig. 4(b): From the bifurcation point (open circle in the

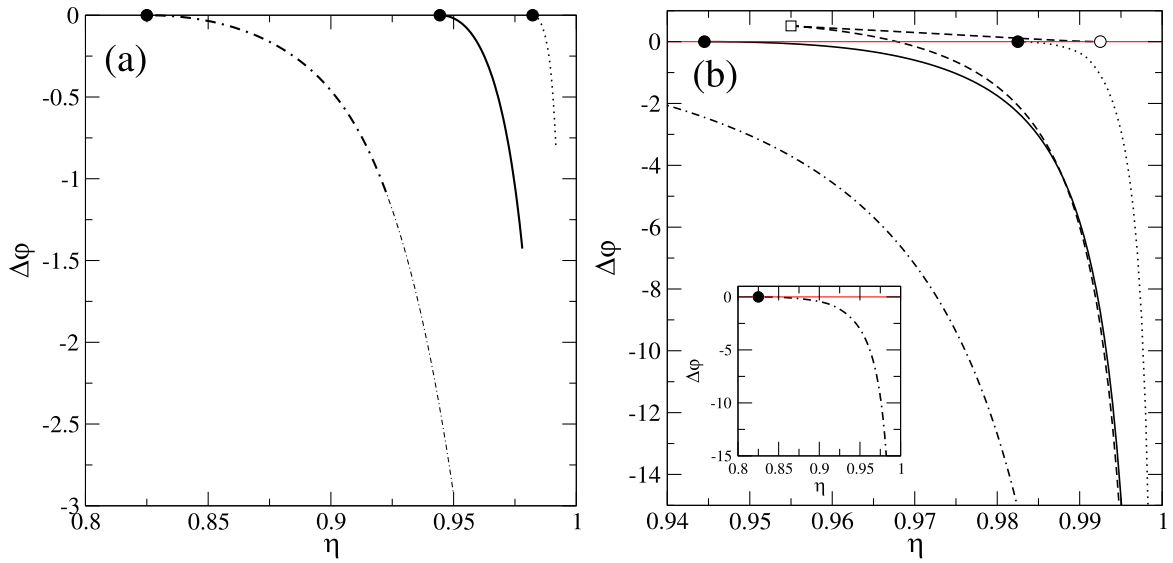

FIG. 4. Free-energy differences $\Delta\varphi \equiv \varphi_\alpha - \varphi_I$, with α= 2-atic (dot-dashed), 8-atic (solid), 4-atic (dashed), and 6-atic (dotted), as a function of packing fraction η, obtained from (a) the Fourier-coefficient method and (b) the one-parameter minimizations. In (a), the dot-dashed line with a shorter step is a simple extrapolation of the 2-atic branch to higher densities. The inset in (b) shows the complete 2-atic branch. Filled circles in (a) and (b) show the bifurcation points at second-order transitions, while the open circle in (b) indicates the first-order counterpart in the 4-atic branch. The open square is the location of the first metastable solution with 4-atic symmetry.

figure), located at a packing fraction $\eta = 0.9928$ (see Table I), an unstable 4-atic branch departs towards lower densities, with a free energy higher than that of the I phase. This branch terminates at $\eta \approx 0.955$ (open square in the figure), where the 4-atic phase becomes metastable for the first time, with a high order parameter Q_4. From this point, a second T branch develops towards higher densities, $\Delta\varphi$ eventually becoming negative at $\eta \simeq 0.968$, indicating that the 4-atic phase is more stable than the I phase. This is the usual scenario for a first-order phase transition. When η further increases from this value, the 4-atic free-energy branch also crosses the 8-atic branch at $\eta \simeq 0.988$. In any case, the free energy of the 2-atic phase has by far the lowest value, as can be seen in Fig. 4. The crossing of the 4-atic and 8-atic branches at high packing fractions is interesting. It can be understood by invoking the limit value of the scaled second-virial coefficient as $\lambda \to \infty$:

$$\tilde{b}_2^{(n)} \equiv \lim_{\lambda\to\infty} b_2[h] = \frac{1}{2an}\left[\frac{A_{\rm excl}(0)+A_{\rm excl}(\pi)}{2} + \sum_{k=1}^{n-1} A_{\rm excl}\left(\frac{k\pi}{n}\right)\right] - 1. \tag{B3}$$

Inserting the known analytic expression for the excluded area $A_{\rm excl}(\phi)$, we obtain $\tilde{b}_2^{(1)} < \tilde{b}_2^{(2)} \lesssim \tilde{b}_2^{(4)} < \tilde{b}_2^{(3)}$ for the 2-atic ($n = 1$), 4-atic ($n = 2$), 6-atic ($n = 3$), and 8-atic ($n = 4$) symmetries. This explains the reason for the crossing behavior: The double-averaged excluded area with respect to $h(\phi)$ for the 4-atic symmetry, although similar in magnitude, is lower than that obtained for the 8-atic symmetry. Obviously, this occurs only at very high densities, when the orientational order is almost perfect and the above asymptotic expression can be justified. The fact that the free energy of the 8-atic phase is lower than that of the 4-atic phase at lower densities implies that the opposite behavior is true when the orientational distribution function is less sharply peaked. nth-order virial theories with an I-8–atic bifurcation below the I-2–atic one, with the free energy of the former below that of the latter, are expected to support the second scenario: After the I-8-atic bifurcation at high packing fractions, the 4-atic energy branch crosses the 8-atic one, and a 8-atic–4-atic first-order phase transition takes place. However, if the crossing point is relatively close to the I-8–atic bifurcation, the two-phase coexistence might involve the I and the 4-atic phases, as shown by the MC simulations.

[1] P. G. de Gennes, Symp. Faraday Soc. **5**, 16 (1971).
[2] U. Tkalec and I. Muševič, Soft Matter **9**, 8140 (2013).
[3] D. Frenkel and B. M. Mulder, Mol. Phys. **55**, 1171 (1985).
[4] D. Frenkel and R. Eppenga, Phys. Rev. A **31**, 1776 (1985).
[5] J. A. Cuesta and D. Frenkel, Phys. Rev. A **42**, 2126 (1990).
[6] G. Bautista-Carbajal and G. Odriozola, J. Chem. Phys. **140**, 204502 (2014).
[7] M. Kleman and G. Ryschenkow, J. Chem. Phys. **64**, 413 (1976).
[8] H. H. Wensink and R. L. C. Vink, J. Phys.: Condens. Matter **19**, 466109 (2007).
[9] H. Schlacken, H.-J. Mogel, and P. Schiller, Mol. Phys. **93**, 777 (1998).
[10] Y. Martínez-Ratón, E. Velasco, and L. Mederos, J. Chem. Phys. **122**, 064903 (2005).
[11] R. Wittmann, C. E. Sitta, F. Smallenburg, and H. Lowën, J. Chem. Phys. **147**, 134908 (2017).
[12] Y. Martínez-Ratón and E. Velasco, Phys. Fluids **34**, 037110 (2022).
[13] Y. Geigenfeind, S. Rosenzweig, M. Schmidt, and D. de las Heras, J. Chem. Phys. **142**, 174701 (2015).
[14] D. A. Triplett and K. A. Fitchhorn, Phys. Rev. E **77**, 011707 (2008).
[15] C. Avendaño and F. A. Escobedo, Soft Matter **8**, 4675 (2012).
[16] S. Mizani, P. Gurin, R. Aliabadi, H. Salehi, and S. Varga, J. Chem. Phys. **153**, 034501 (2020).
[17] J. A. Martínez-González, J. C. Armas-Pérez, and J. Quintana-H, J. Stat. Phys. **150**, 559 (2013).
[18] P. A. Monderkamp, R. S. Windisch, R. Wittmann, and H. Löwen, J. Chem. Phys. **158**, 164505 (2023).
[19] J. P. Ramírez González and G. Cinacchi, Phys. Rev. E **102**, 042903 (2020).
[20] K. Zhao, C. Harrison, D. Huse, W. B. Russel, and P. M. Chaikin, Phys. Rev. E **76**, 040401(R) (2007).
[21] K. Zhao, R. Bruinsma, and T. G. Mason, Proc. Natl. Acad. Sci. USA **108**, 2684 (2011).
[22] K. Zhao, R. Bruisma, and T. G. Mason, Nat. Commun. **3**, 801 (2012).
[23] J. A. Anderson, J. Antonaglia, J. A. Millan, M. Engel, and S. C. Glotzer, Phys. Rev. X **7**, 021001 (2017).
[24] C. H. Mak, Phys. Rev. E **73**, 065104(R) (2006).
[25] B. P. Prajwal and F. A. Escobedo, Phys. Rev. Mater. **5**, 024003 (2021).
[26] T. Geigenfeind and D. de las Heras, J. Chem. Phys. **150**, 184906 (2019).
[27] Y. Martínez-Ratón and E. Velasco, Phys. Rev. E **79**, 011711 (2009).
[28] T. Müller, D. de las Heras, I. Rehberg, and K. Huang, Phys. Rev. E **91**, 062207 (2015).
[29] M. González-Pinto, F. Borondo, Y. Martínez-Ratón, and E. Velasco, Soft Matter **13**, 2571 (2017).
[30] Z. Hou, Y. Zong, Z. Sun, F. Ye, T. G. Mason, and K. Zhao, Nat. Commun. **11**, 2064 (2020).
[31] Y. Martínez-Ratón and E. Velasco, Phys. Rev. E **102**, 052128 (2020).
[32] Y. Martínez-Ratón, E. Velasco, and L. Mederos, J. Chem. Phys. **125**, 014501 (2006).
[33] Y. Martínez-Ratón and E. Velasco, Phys. Rev. E **104**, 054132 (2021).
[34] A. P. Gantapara, W. Qi, and M. Dijkstra, Soft Matter **11**, 8684 (2015).
[35] P. Padilla and E. Velasco, J. Chem. Phys. **106**, 10299 (1997).
[36] F. H. Ree and W. G. Hoover, J. Chem. Phys. **40**, 939 (1964).